bioRxiv preprint doi: https://doi.org/10.1101/2022.10.20.513108; this version posted October 21, 2022. The copyright holder for this preprint (which was not certified by peer review) is the author/funder, who has granted bioRxiv a license to display the preprint in perpetuity. It is made available under aCC-BY-NC-ND 4.0 International license.

Title: Intra-V1 functional networks predict observed stimuli

Authors: Marlis Ontivero-Ortega[1,2]*, Jorge Iglesias-Fuster[1], Daniele Marinazzo[2], Mitchell Valdes-Sosa[1,3]

Affiliations: [1] Cuban Center for Neuroscience, Havana, Cuba

[2] Psychology, Faculty, Ghent University, Belgium

[3] The Clinical Hospital of Chengdu Brain Sciences, University of Electronic Sciences Technology of China, Chengdu, China

Author Note

*Corresponding author, email: luna@cneuro.edu.cu

bioRxiv preprint doi: https://doi.org/10.1101/2022.10.20.513108; this version posted October 21, 2022. The copyright holder for this preprint (which was not certified by peer review) is the author/funder, who has granted bioRxiv a license to display the preprint in perpetuity. It is made available under aCC-BY-NC-ND 4.0 International license.

Abstract

A recent fMRI study found that the patterns of fMRI co-fluctuations within V1 changed with variations in the perceptual organization of observed stimuli. Intra-V1 correlation matrices associated with modified Global and Local Navon letters (that allowed dissociation of levels over time) were examined with univariate tests. Links between left/right V1 areas were found for Global letters, whereas links for Local letters were concentrated within the left dorsal V1. Here we used multivariate pattern analysis on the same data to predict the level and shape of the observed Navon letter from V1 correlation matrices to ascertain the stability across subjects of network topologies and if they contained invariant information about shape or level. We found that inter-subject classification was accurate for both level and letter shape. Intra-participant cross-classification of levels across shape was accurate but failed for shape across levels. Furthermore, cross-classification weight maps evinced asymmetries of link strengths across the visual field that mirrored perceptual asymmetries. These results indicate that the association of V1 topologies and perceptual states is stable across participants. We hypothesize that feedback (that differs between level and shape) to V1 drives the intra-V1 networks and that the topology of intra-V1 networks can shed light on the neural basis of perceptual organization.

Keywords: V1, fMRI, functional networks, SVM-classifier, Navon task, weight-maps

bioRxiv preprint doi: https://doi.org/10.1101/2022.10.20.513108; this version posted October 21, 2022. The copyright holder for this preprint (which was not certified by peer review) is the author/funder, who has granted bioRxiv a license to display the preprint in perpetuity. It is made available under aCC-BY-NC-ND 4.0 International license.

Introduction

The function of cortical areas is determined not only by their input/output connections but also by their internal neural circuitry. Therefore, much information is missed when the functional magnetic resonance imaging (fMRI) time series of a region are averaged. This averaging is common in several studies of brain-wide networks, in which cortical areas are seen as unitary nodes in networks and represented by the mean of fMRI activity of all voxels or vertices inside the region (Schaefer et al., 2018; Sporns & Betzel, 2016). By collapsing voxels, we overlook potential signs of neural cooperation -indexed by co-fluctuations of neuronal activity- within cortical regions. Also, many studies of functional connectivity use resting state fMRI. However, task-fMRI connectivity is gaining increased attention, which is more sensitive to behaviour and allows better mapping of specific cognitive functions (Finn, 2021). The primary visual cortex (V1) is a good candidate for studying its internal connectivity during tasks since much is known about its internal specialization and neural circuitry (Saenz & Fine, 2010; Seidemann & Geisler, 2018). There is also a close correspondence between its macroscopic anatomy and retinotopic organization (Benson et al., 2012; Benson & Winawer, 2018), simplifying comparisons across individuals. Furthermore, given the small size of its population receptive fields (pRFs, Wandell & Winawer, 2015), synchronization of neural activity in V1 over long visual field distances would imply either internal lateral interactions (Chen et al., 2014) or feedback from high-order visual areas (Lamme & Roelfsema, 2000; Liang et al., 2017).

Therefore, it seems worthwhile to search for associations between patterns of intra-V1 fMRI connectivity and cognitive processes. To our knowledge, only two studies have attempted to address this directly, both focusing on the perceptual organization of visual scenes. These works (Nasr et al., 2021; Valdes-Sosa et al., 2022) found that fMRI co-fluctuations in V1 change over a large spatial scale as the perceptual organization of observed

bioRxiv preprint doi: https://doi.org/10.1101/2022.10.20.513108; this version posted October 21, 2022. The copyright holder for this preprint (which was not certified by peer review) is the author/funder, who has granted bioRxiv a license to display the preprint in perpetuity. It is made available under aCC-BY-NC-ND 4.0 International license.

stimuli varies. Previous work on intra-V1 connectivity with resting-state fMRI had focused on structural (task-invariant) factors as the geodesic distance between cortical sites (Dawson et al., 2016). Although fMRI probably reflects only a subset of the interactions within V1 (due to spatial and temporal resolution restrictions), it has been applied to study medium-scale (intra-nodal) interactions between different visual areas (Baldassano et al., 2012; Haak et al., 2013).

Valdes-Sosa et al. reported that V1 network topologies associated with Global and Local Navon letters were strikingly different. They used a novel stimulation approach (Iglesias-Fuster et al., 2014). In traditional Navon figures, both hierarchical levels are presented simultaneously. In the modified Navon figures, each level emerges from a background mask at different times (see Figure 1). This temporal segregation allows measuring distinct fMRI responses for the two levels and permits orthogonality with letter shape in the design. A higher number of links (connections) were found between the left/right V1 areas for Global, compared to Local letters. Congruently, Nasr et al. also found stronger connectivity between regions of interest (ROIs) in the left/right V1 when they mapped parts of the same object instead of pieces of different objects. In both studies, these interhemispheric links were stronger in the dorsal V1 region (corresponding to the lower visual hemifield), which is consistent with an advantage for global perception in the lower visual field in psychophysical studies (Levine & McAnany, 2005). Valdes-Sosa et al. also found that links associated with Local letters were concentrated in the left dorsal V1 (lower right visual quadrant), which mirrors a left hemisphere superiority for Local Navon letters found in neuropsychological and psychophysical reports (Flevaris & Robertson, 2016).

The two studies described above used repeated-measures univariate statistical hypothesis testing. In one case (Nasr et al., 2021), a small number of V1 ROIs were selected. In the other study (Valdes-Sosa et al., 2022), massive edgewise tests or network-based

bioRxiv preprint doi: https://doi.org/10.1101/2022.10.20.513108; this version posted October 21, 2022. The copyright holder for this preprint (which was not certified by peer review) is the author/funder, who has granted bioRxiv a license to display the preprint in perpetuity. It is made available under aCC-BY-NC-ND 4.0 International license.

statistics were employed (followed by multiple-comparisons corrections). It would be interesting to examine if multivariate characterizations of V1 network topology also vary with, or are even more sensitive to, the effects of perceptual organization. Since univariate testing ignores systematic associations between different features, more complex patterns are possibly missed. Moreover, significant within-subject effects -although informative- do not address the stability of network topologies across individuals, which is especially relevant in studies with a small number of participants (Calhoun, 2022). Finally, hypothesis testing (by itself) does not enable predictions (diagnosis) for individual cases (Bzdok & Ioannidis, 2019).

We speak to these issues using MVPA techniques on the fMRI connectivity matrices from the Valdes-Sosa et al. study. MVPA examines differences between conditions (Davis & Poldrack, 2013; Haynes & Rees, 2006) by combining information across measurement units (in our case, network links). Inter-subject MVPA (Wang et al., 2020) can answer the question about the stability of network topology across individuals. In this procedure, training data from some individuals are used to build a classifier to test data from other individuals. Above-chance accuracy in inter-subject classification bolsters conclusions from small sample studies and explores the possibility of predictions for new individuals. Despite some limitations of the inter-subject MVPA methodology, its use is facilitated for intra-V1 data, given the excellent inter-subject registration of the retinotopic mapping for this region (Benson & Winawer, 2018).

We also used MVPA to examine which visual attributes are related to V1 network topology while exhibiting tolerance for changes in other attributes. On the one hand, V1 network topology could reflect the spatial scale used to integrate the relevant stimuli. For example, Global letters integrate across bigger chunks of the visual field than Local letters, which could be independent of their shape (Han & Humphreys, 1999, 2002). On the other hand, V1 network topology could reflect the specific arrangement of contours defining the

bioRxiv preprint doi: https://doi.org/10.1101/2022.10.20.513108; this version posted October 21, 2022. The copyright holder for this preprint (which was not certified by peer review) is the author/funder, who has granted bioRxiv a license to display the preprint in perpetuity. It is made available under aCC-BY-NC-ND 4.0 International license.

letter's shape, perhaps at more than one spatial scale. Scale-free shape information is available in areas coding shapes with size invariance (such as the lateral occipital complex or LOC; Grill-Spector, 2003). The invariance of neural patterns associated with one feature with respect to another can be tested with MVPA cross-classification (Kaplan et al., 2015). Cross-classifiers are trained to discriminate for attribute A at one Level of feature B (e.g., shape at the Global Level), then are tested to discriminate for attribute A at another value of B (e.g., shape at the Local Level). The success of this learning transfer implies that neural representations for A are tolerant to changes in B (that is, shape information is invariant to level, which is more abstract).

Additionally, the retinotopic organization of V1 allows meaningful interpretation of the feature weight maps underlying successful classifiers in the visual field. V1 network edges connect cortical sites for which population receptive fields (pRFs) have been mapped (Wandell & Winawer, 2011, 2015). The weight of each link can thus be plotted in the visual field as a line connecting the positions (defined by the pRFs) corresponding to two nodes. The network edges contributing most to the predictions should have a characteristic spatial pattern, corresponding to the stimulus properties, in the visual field.

To sum up, here we re-analyzed data from our previous work (Valdes-Sosa et al. 2022) to answer the following questions: 1) Is it possible to train inter-subject classifiers based on V1 correlation matrices to accurately predict in new subjects the hierarchical level and shape of observed Navon letters? 2) Is it possible to perform accurate intra-subject cross-classification of observed letter shapes tolerant to changes in level and presented levels tolerant to changes in letter shape? 3) What is the retinotopic distribution of the features that contribute most to the accuracy of the classifiers in the previous questions?

bioRxiv preprint doi: https://doi.org/10.1101/2022.10.20.513108; this version posted October 21, 2022. The copyright holder for this preprint (which was not certified by peer review) is the author/funder, who has granted bioRxiv a license to display the preprint in perpetuity. It is made available under aCC-BY-NC-ND 4.0 International license.

Materials and Methods

The data used here have been previously described in other publications. A summary description is provided below; see Valdés-Sosa et al., 2020 and Valdés-Sosa et al., 2022, for a full explanation.

Participants

Twenty-six human volunteers (ages 23 to 28 years; 9 females) participated in the study. All had normal, or corrected-to-normal, vision, did not present any medical condition and were right-handed except for two cases. The procedures were approved by the ethics committee of the University for Electronic Science and Technology of China (UESTC), and participants gave written informed consent in compliance with the Helsinki declaration.

Stimuli and tasks

Modified Navon figures (Figure 1) were presented in the experiment. Two letters, E and U, were presented at both levels in a blocked stimulus paradigm. The 1 s letter presentation alternated with a background mask also flashed for 1 s. The letters were made from white lines on a black background (about 2.0° wide and 5.3° high). This matrix was built out of smaller placeholder elements shaped like '8's (with visual angles about 40' wide and 1° 3' high). Only one letter was shown in each block, in which participants were required to report the number of minor deviations in letter shape. The stimuli were projected on a screen at the subject's feet, viewed through an angled mirror fixed to the MRI head-coil, and were generated using the Cogent Matlab toolbox (http://www.vislab.ucl.ac.uk/cogent.php).

Blocks had 44 sec of duration and consisted of an initial cue ('Global' or 'Local') (1 s), followed by a 19-sec baseline, 20 s of the same letter (1-sec repetition) and were ended with a 4 sec wait period where the number of shape deviations was reported. Five runs were presented in 24 participants and four runs in two, each consisting of 12 blocks (3 blocks for each letter: EG, EL, UG, and UL).

bioRxiv preprint doi: https://doi.org/10.1101/2022.10.20.513108; this version posted October 21, 2022. The copyright holder for this preprint (which was not certified by peer review) is the author/funder, who has granted bioRxiv a license to display the preprint in perpetuity. It is made available under aCC-BY-NC-ND 4.0 International license.

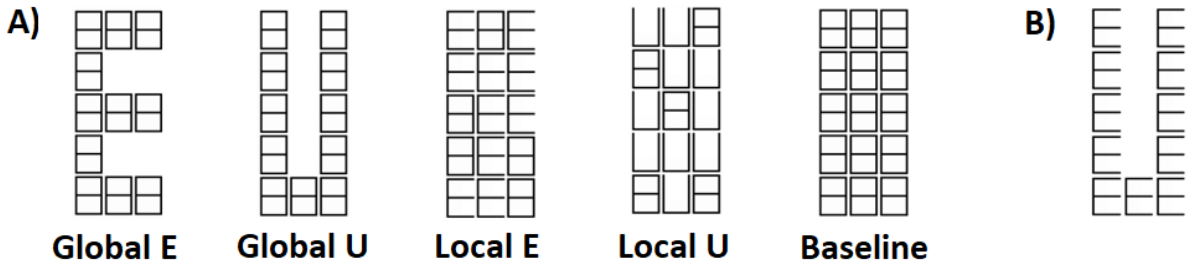

Figure 1: Navon figures. A) Modified figures used in the experiment. Two letters (E and U), and two levels (Global and Local). B) Example of traditional Navon figure.

Data acquisition and Image pre-processing

Recordings were carried out with a GE Discovery MR750 3T scanner (General Electric Medical Systems, Milwaukee, WI, USA) using an eight-channel receiver head coil. Functional images were obtained with a T2*- weighted echo planar imaging sequence (TR=2.5s; TE=40 ms; flip angle=90°) with a spatial resolution of 1.875 x 1.875 x 2.9 and 135 images per run. A T1-weighted image was also obtained with 1 x 1 x 0.5 mm resolution.

Initial pre-preprocessing of functional data included discarding the first five volumes of fMRI in all runs, artifact correction (using ArtRepair toolbox (http://cibsr.stanford.edu/tools/ArtRepair/ArtRepair.htm), followed by slice-timing, head motion correction (with the extraction of motion parameters) and unwarping with SPM8 (http://www.fil.ion.ucl.ac.uk/spm/). The T1 Image was segmented and normalized to MNI space using SPM12 to extract nuisance parameters from fMRI activity in white matter (WM), and cerebrospinal fluid (CSF) that were included in the general linear model described below. For each subject, these masks were created using a threshold of tissue probability greater than 0.9. The CSF mask was also restricted to the ventricles using a template in MNI space (https://sites.google.com/site/mrilateralventricle/template).

Cortical surfaces (white and pial) were reconstructed from the T1 Image for each subject using Freesurfer (http://surfer.nmr.mgh.harvard.edu), registered to the FsAverage template, and subsampled to 81924 vertices. The mid-gray cortical surface was co-registered

bioRxiv preprint doi: https://doi.org/10.1101/2022.10.20.513108; this version posted October 21, 2022. The copyright holder for this preprint (which was not certified by peer review) is the author/funder, who has granted bioRxiv a license to display the preprint in perpetuity. It is made available under aCC-BY-NC-ND 4.0 International license.

with the functional data. Then the fMRI time series were interpolated to each mid-gray cortical surface and high-pass filtered with a time constant of 128 s. Also, for subsequent spatial smoothing of the functional data in V1, discs with 5mm radii were defined over the FsAverage surface using the Surfing toolbox (http://surfing.sourceforget.net).

Estimation of fMRI background activity connectivity matrices

Background activity (BA) was defined as the residual time series of each surface vertex after regressing out the effects of the stimuli (evoked response) and 64 nuisance parameters (a standard set of nuisance variables to eliminate the effects of noise, artifacts, and physiological contaminants) applying a general linear model (GLM). The nuisance regressors included the primary motion parameters, their derivatives, and the quadratics of both these sets (24 motion regressors in total). Physiologic noise was modeled using the aCompCor method (Behzadi et al., 2007) on the time series extracted separately from the masks of WM and CSF in ventricles in volume space. The first five principal components from each set of time series, the derivatives of these components, and the quadratics of all these parameters were obtained (40 regressors in total). For the GLM, each stimulation block was modeled as a square wave convolved with the canonical hemodynamic function.

The residual time series in V1 vertices, obtained after GLM, were smoothed by averaging with the time series of its neighbours in the 5 mm discs mentioned above. The studied V1 region was restricted to the central 8 degrees of eccentricity in a probabilistic a priori map (Benson & Winawer, 2018). Next, the time series were segmented into blocks considering the time shift introduced by the hemodynamic function. These segments were linearly detrended, and segments corresponding to the same stimulus were concatenated.

Finally, the internal V1 connectivity matrices of BA were estimated by calculating the Pearson correlation coefficient between the time series for each vertex of V1 and segregated by stimulus condition (EG, EL, UG, UL) in all participants. For the classification analysis, all

bioRxiv preprint doi: https://doi.org/10.1101/2022.10.20.513108; this version posted October 21, 2022. The copyright holder for this preprint (which was not certified by peer review) is the author/funder, who has granted bioRxiv a license to display the preprint in perpetuity. It is made available under aCC-BY-NC-ND 4.0 International license.

matrices were vectorized. The correlation values were converted to z-values using the Fisher transformation, negative values were set to zero, and missing values in each subject's vector were substituted by the median value of the other participants without missing values. These missing values could have been due to noise or BOLD signal dropout at specific cortical vertices. However, they were few and concentrated in restricted areas of the visual field (see Figure 10 in Valdes-Sosa et al., 2022).

Classification analysis

Intersubject MVPA (to assess stability across participants) and within-subject cross-classification MVPA (to assess discrimination invariance) were performed, in which the possibility of predicting observed stimuli from the intra-V1 connectivity matrices was measured. In all tests, the connection strengths between all node pairs were used as features, and a support vector machine (SVM) was used as the classifier (with the default parameter C=1). Feature selection was performed to eliminate some irrelevant connections by applying a two-tailed t-test between conditions on the training data and retaining links with significant t-values ($p < 0.01$). Prediction accuracy (Acc) and the area under the ROC curve (AUC) were used to assess the performance of each classifier. The statistical significance of deviation from a random classification (0.5 for Acc and AUC) was estimated by permutation testing (nperm=1000), in which stimulus labels were randomly changed (Valente et al., 2021).

Intersubject-classification

Specific inter-subject classification tests were performed to evaluate if the pattern of association between stimulus conditions and V1 network topology was stable across participants. These tests were carried out with cross-validation in a leave-one-subject-out (LOSO). Thus, training was based on the data of n-1 participants and testing on the data of the remaining participant. The four discriminations tested were Level (Global vs Local), separately for the 'E' and the 'U' stimuli, and letter shape ('E' vs 'U'), separately for the Global

bioRxiv preprint doi: https://doi.org/10.1101/2022.10.20.513108; this version posted October 21, 2022. The copyright holder for this preprint (which was not certified by peer review) is the author/funder, who has granted bioRxiv a license to display the preprint in perpetuity. It is made available under aCC-BY-NC-ND 4.0 International license.

and the Local stimuli. Each iteration of the LOSO consisted of 50 training samples and two testing samples.

Cross-classification

Cross-classification tests were employed to see if models built for one relevant feature (e.g., level) were invariant to changes in another irrelevant feature (e.g., letter identity). The data from all subjects were divided into two sets of pairs (each with 52 observations) to test the invariance of level discrimination with respect to letter identity: those associated with EG-EL, and with UG-UL. The data was also divided into matrices associated with EG-UG and EL-UL to test the invariance of letter discrimination with respect to level. The classifier was trained alternating which pair was used for training and which for testing, and the two accuracies and AUCs were averaged and reported. Thus, two instances of the cross-classifier were always calculated (e.g., Level for 'E' and 'U'). Note that cross-validation was unnecessary in these tests since the classifier was trained with data from one pair of conditions and tested with independent data from the other pair. Permutation tests were based on randomizing the labels of the training data in both directions of the test, with the resulting p-values combined with Fisher's method.

Analysis of weight maps in the Cross-classifications

The weight maps of the SVM cross-classifiers were examined to determine which regions of V1 contributed most to classification tests. This analysis was not carried out for the specific intersubject tests since their weight maps are necessarily different, reflecting the retinotopic pattern of stimulation. In contrast, the invariance of weight maps for one attribute despite changes in another implies a generalization beyond the precise pattern of retinotopic stimulation.

The stability of the weight maps was estimated by bootstrapping (nboot=1000). In each bootstrap iteration, new data was created by resampling with replacement across

bioRxiv preprint doi: https://doi.org/10.1101/2022.10.20.513108; this version posted October 21, 2022. The copyright holder for this preprint (which was not certified by peer review) is the author/funder, who has granted bioRxiv a license to display the preprint in perpetuity. It is made available under aCC-BY-NC-ND 4.0 International license.

participants. The SVM was re-trained in each replication to obtain multiple models (for both instances of the irrelevant attribute). The estimated model coefficients were transformed into forward models ("activation" maps) as proposed by Haufe (Haufe et al., 2014) to enhance the interpretability of these transformed maps (HTW) and allow assessment of their stability.

We then calculated the concordance of HTW map feature rankings between the two instances of the invariant cross-classifications. If the classifiers trained separately for two instances yield similar weight maps, then the features guiding the generalization of learning across the two situations are equivalent. Concordance was measured between the two instances for each bootstrap replicate using Kendall's W index (which ranges from 0 for no concordance to 1 for perfect concordance). If the classifiers contain invariant information (tolerant to changes in the irrelevant feature), the ranking of activations in the two HTW maps should be highly concordant. The 95 % bias-corrected and accelerated percentile confidence intervals were calculated with the W bootstrapped samples.

The HTW maps from the two cross-classification instances were averaged to enhance features that were relevant in both. This average HTW map was transformed into a robust pseudo-zscore (https://github.com/cvnlab/knkutils), obtained by dividing the median of the feature by one-half the width of the central 68% range (an analog of a standard error) of the bootstrap values. This Z-transformed HTW map was split into positive and negative portions (e.g., each favouring one level). The absolute values of these maps were fit with two models: a gaussian distribution and the mixture of a null gaussian and gamma distribution. The model with the lowest Bayesian information criterion (BIC) was used to estimate the respective false discovery rates (q=0.00001). Finally, the pseudo-zscores (representing edges in a connectivity matrix) surviving the FDR threshold were projected onto the visual field and shown as graph plots in visual field coordinates, using the mean polar angles and

bioRxiv preprint doi: https://doi.org/10.1101/2022.10.20.513108; this version posted October 21, 2022. The copyright holder for this preprint (which was not certified by peer review) is the author/funder, who has granted bioRxiv a license to display the preprint in perpetuity. It is made available under aCC-BY-NC-ND 4.0 International license.

eccentricities for V1 vertices extracted from a population retinotopy prior map (Benson & Winawer., 2018).

We also calculated the 95 % percentile confidence intervals for each feature in the average HTW map. Significant features (links for which the confidence interval did not include zero) were plotted within the original correlation matrix space. Median HTW values were projected as graph plots onto the visual field as indicated above.

Results

The results of accuracy and AUC for all classification tests are shown in Figure 2. In the inter-subject classification, it was possible to accurately decode both specific instances of the classifier level (Acc: 0.79, AUC: 0.89 for 'E' and Acc: 0.75, AUC: 0.85 for 'U') and for letter identity (Acc: 0.73, AUC: 0.83 for Global and Acc: 0.69, AUC: 0.74 for Local). In all cases, the permutation tests were highly significant. Thus, significant inter-subject classification showed that the V1 topologies associated with each stimulus condition were stable across subjects. Note that the retinotopic shape representations in this test are ultimately scale-specific (i.e., global and local instances of the same shape stimulate different retinal sites), and the retinotopic representation of level is letter specific.

Invariant Level cross-classification was highly significant (Acc: 0.70, AUC: 0.82). In contrast, invariant letter cross-classification was at a chance level (Acc: 0.54, AUC: 0.52) and not significant. These results indicate that the spatial scale (invariant to shape) is well reflected in the topology of intra-V1 networks, whereas letter shape independent from spatial scale is not.

bioRxiv preprint doi: https://doi.org/10.1101/2022.10.20.513108; this version posted October 21, 2022. The copyright holder for this preprint (which was not certified by peer review) is the author/funder, who has granted bioRxiv a license to display the preprint in perpetuity. It is made available under aCC-BY-NC-ND 4.0 International license.

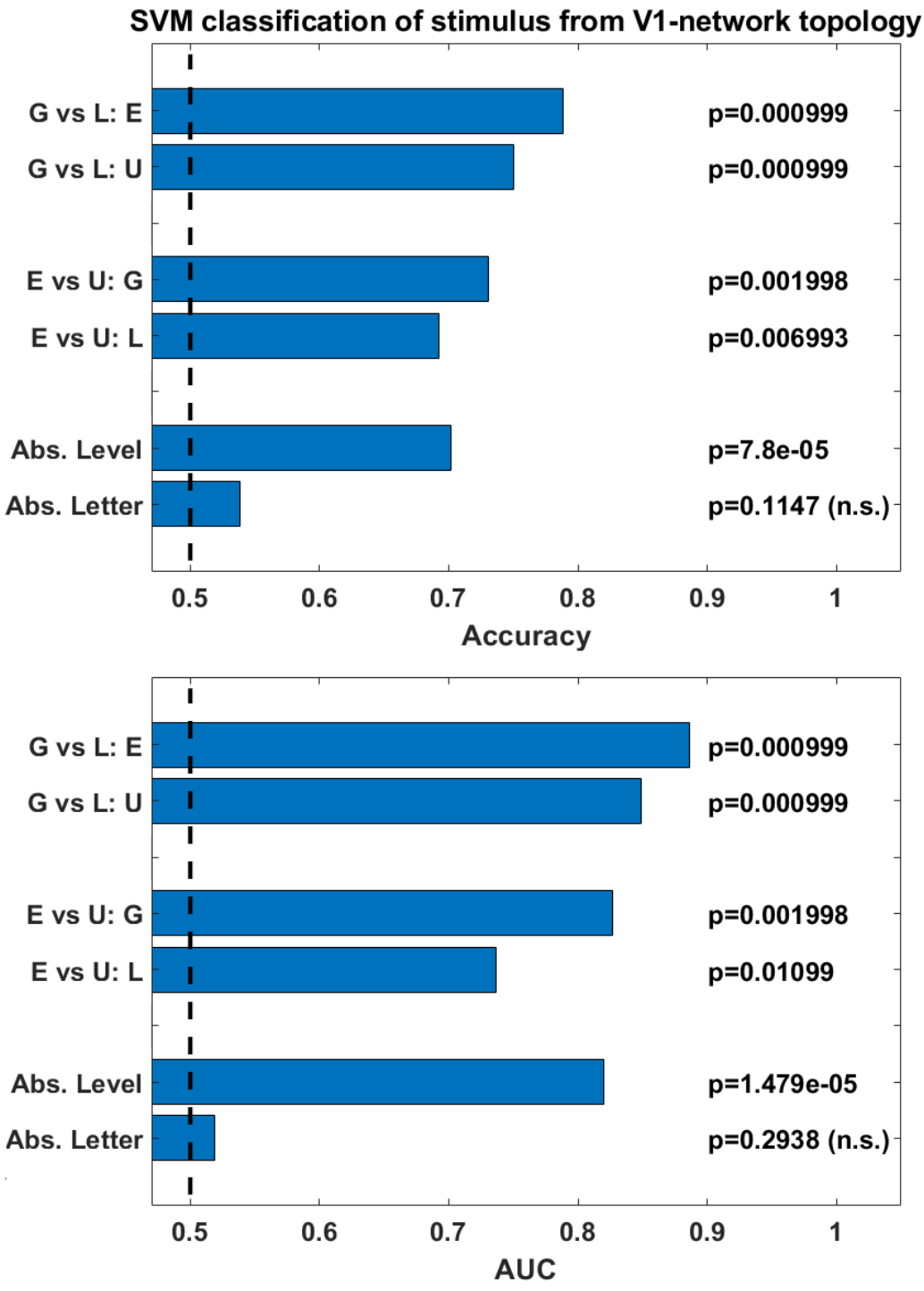

Figure 2: Classifier performance. The upper panel shows accuracy values in the bars. The lower panel shows AUC values in the bars. A vertical dotted line represents the chance level (0.5). Probabilities values from the permutation tests are shown in the numerical insets.

bioRxiv preprint doi: https://doi.org/10.1101/2022.10.20.513108; this version posted October 21, 2022. The copyright holder for this preprint (which was not certified by peer review) is the author/funder, who has granted bioRxiv a license to display the preprint in perpetuity. It is made available under aCC-BY-NC-ND 4.0 International license.

Since accuracy in the cross-classifier for letter identity was at chance, we only show HTW results for level. A comparison of the HTW maps for the classifiers discriminating the Global/Local 'E' and for the Global/Local letter 'U' shows that they were very similar. The observed W values between the two intra-subject SVM classifiers for level was 0.77, with a 95% BCa confidence interval [0.65-0.83], which was well above zero (see the histogram in Figure 3). This result is congruent with the accurate learning transfer between the two instances of level cross-classifiers.

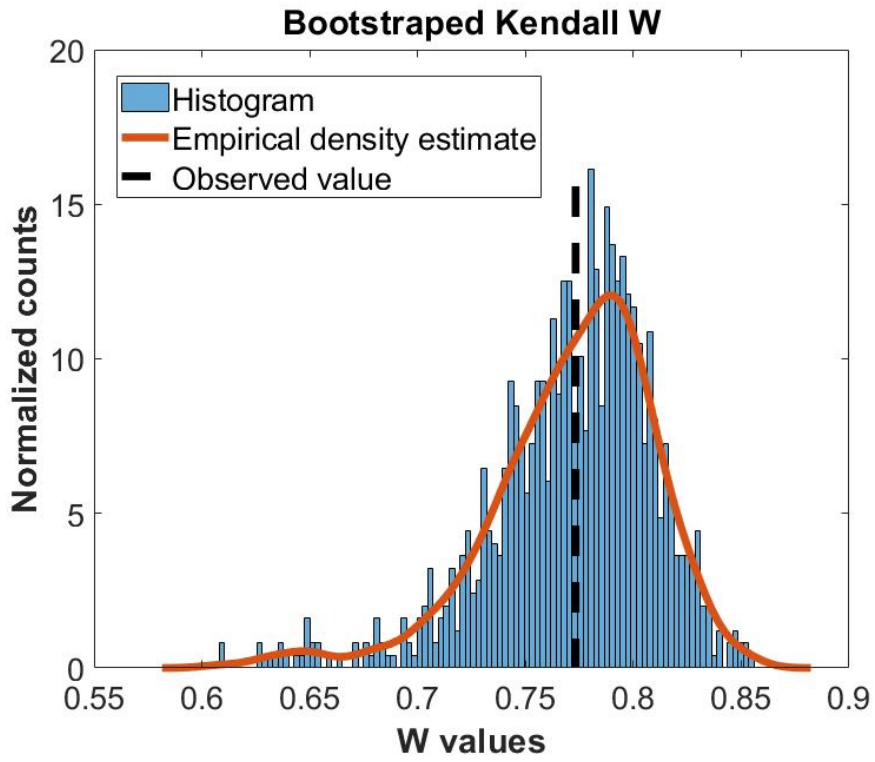

Figure 3: Distribution of bootstrapped Kendall W values. The resampling was over the 26 participants.

Maps of the link pseudo-z scores on the SVM Haufe-transformed weights (HTW) for the invariant level classifiers are plotted in the visual field in Figure 4. The gaussian+gamma mix provided better fits (lower BIC) than the lone gaussian for both positive and negative HTWs. The map for negative HTWs (favouring Global), after thresholding with the FDR

bioRxiv preprint doi: https://doi.org/10.1101/2022.10.20.513108; this version posted October 21, 2022. The copyright holder for this preprint (which was not certified by peer review) is the author/funder, who has granted bioRxiv a license to display the preprint in perpetuity. It is made available under aCC-BY-NC-ND 4.0 International license.

calculated from the distribution mixture fit, exhibits many links crossing the vertical meridian, mainly in the lower visual field. The map for positive HTWs (favouring Local) shows many links circumscribed to the lower right and left visual quadrants.

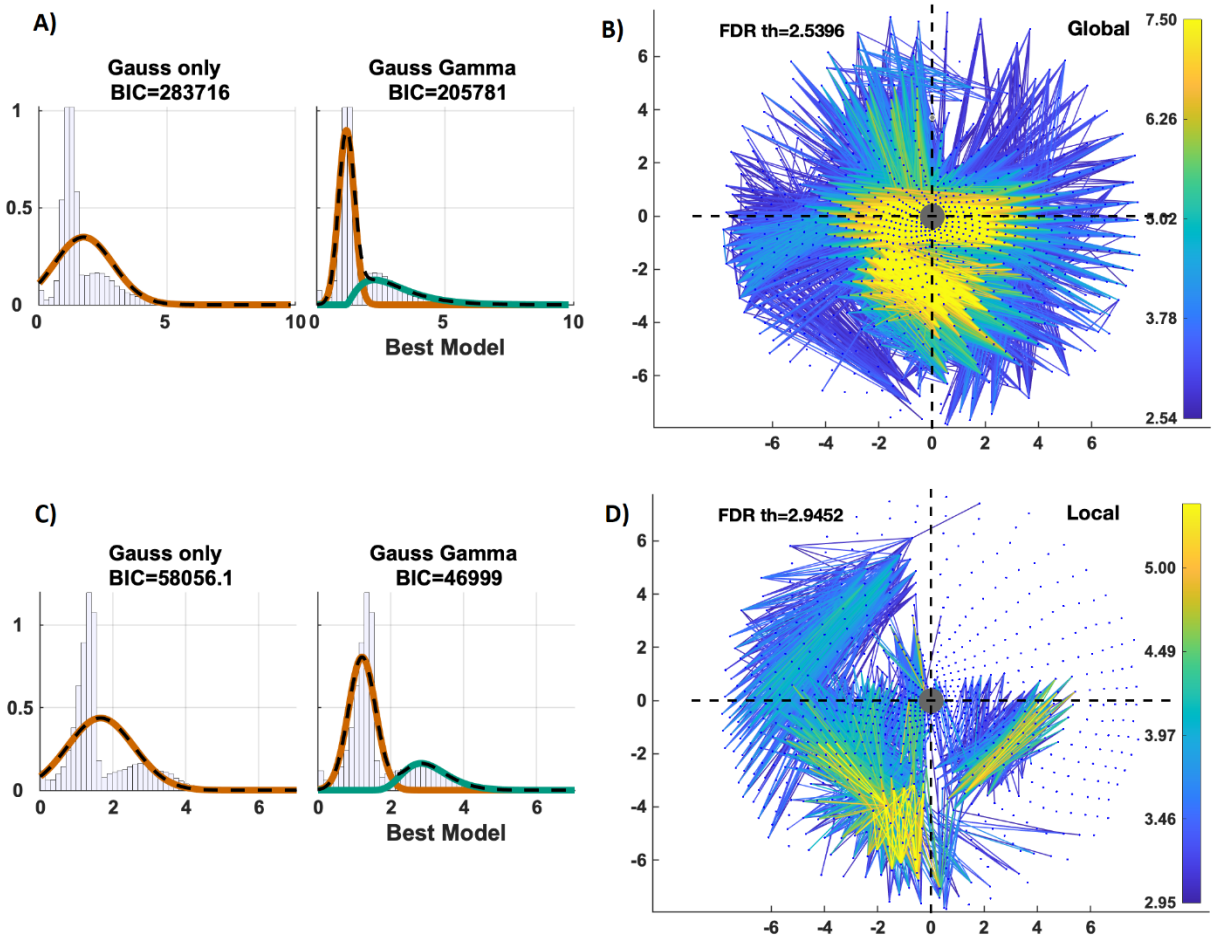

Figure 4. Analysis of standardized SVM Haufe-transformed weight (HTW) maps for the invariant level classifiers. The top row (A, B) corresponds to negative HTWs (indicating Global, although absolute values are shown), and the bottom row (C, D) corresponds to positive HTWs (indicating Local). The distribution mixture fits are shown on the left side of the figure, with data histograms in black, the gaussian component in red, and the gamma component in green. On the right side, graph plots in the visual field of the features surviving the FDR threshold, with colour representing the magnitude of the pseudo-zscores. The gray circle represents the center of gaze, x and y axis represent degrees. Each light-blue dot corresponds to the center of a V1 pRF in the visual field.

Congruent results were obtained for the confidence interval analysis based on the HTW bootstrap. The links with confidence intervals that did not include zero are shown in

bioRxiv preprint doi: https://doi.org/10.1101/2022.10.20.513108; this version posted October 21, 2022. The copyright holder for this preprint (which was not certified by peer review) is the author/funder, who has granted bioRxiv a license to display the preprint in perpetuity. It is made available under aCC-BY-NC-ND 4.0 International license.

Figure 5 (corresponding to values above chance). In this correlation matrix space, interhemispheric links dominate in the Global condition (occupying the block anti-diagonal), whereas intrahemispheric links dominate in the Local condition (occupying the block anti-diagonal). When projected onto the visual space, the median values of significant HWT values tend to cross the vertical meridian of the VF in the lower quadrants for the Global condition. Significant HWT values in the Local condition tend to stay within single visual field quadrants, especially the lower ones. These results are largely congruent with the findings in Figure 4.

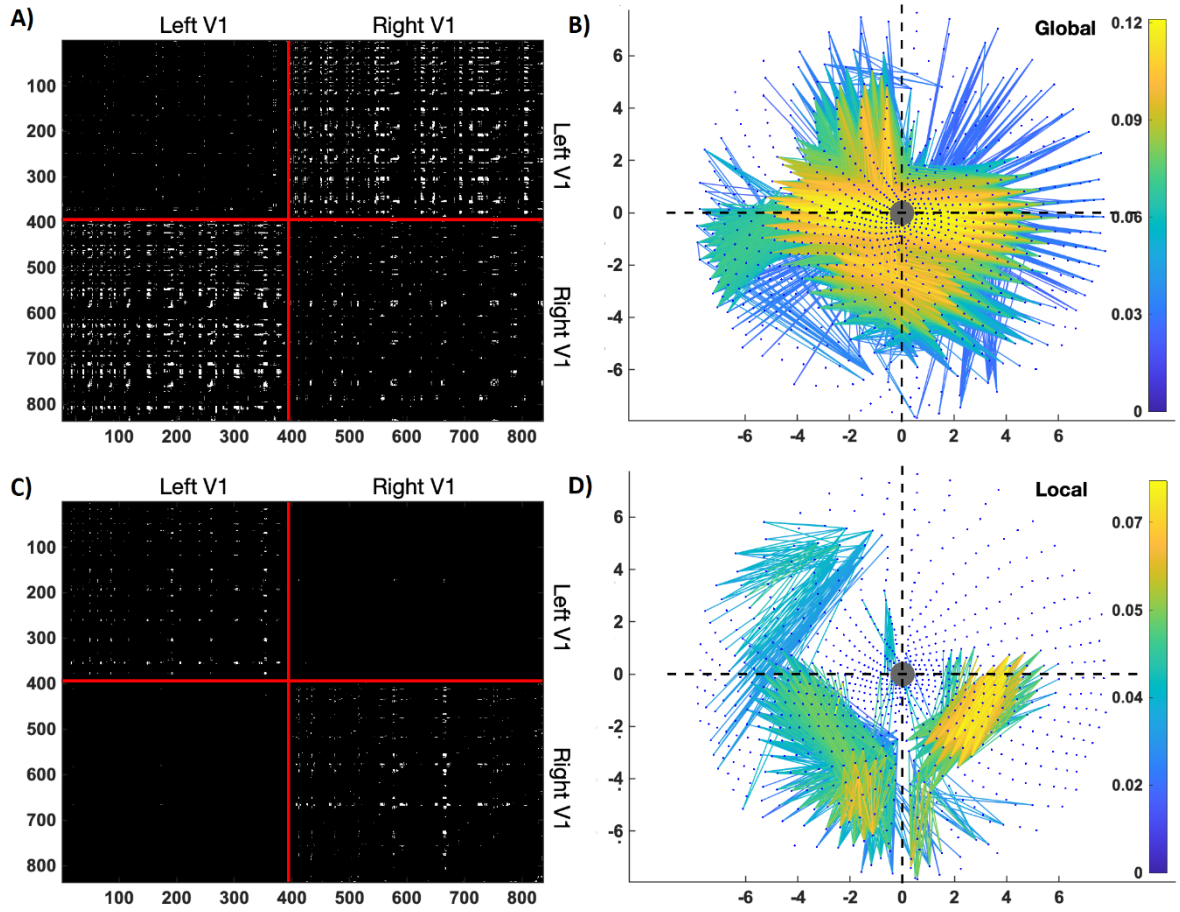

Figure 5. Confidence Intervals (95%) analyses of Haufe-transformed weight maps for the invariant level classifier. Cases in which the intervals did not contain zero were selected and plotted separately for positive activations (top row: A, B) and negative activations (bottom row: C, D). On the left, the surviving features are marked in white within the original V1 vertex correlation matrices. The numbers on the axis indicate the position in an arbitrary list of V1 cortical vertices. The red lines indicate where the list of vertices transitions from the left to the right V1. On the right side of the figure, the median HWT of surviving features

bioRxiv preprint doi: https://doi.org/10.1101/2022.10.20.513108; this version posted October 21, 2022. The copyright holder for this preprint (which was not certified by peer review) is the author/funder, who has granted bioRxiv a license to display the preprint in perpetuity. It is made available under aCC-BY-NC-ND 4.0 International license.

are displayed in graph plots projected into the visual field, with the same conventions as in figure 4.

Discussion

Prediction of the observed stimuli from intra-V1 correlation matrices (corresponding to their associated fMRI time-widows) was highly accurate in the two multivariate analyses carried out in this article. First, four types of specific discriminations accurately predicted which stimuli one participant had observed after training it on the data from the other participants. This classification was accurate when discriminating both stimulus level (Global/Local for both the 'E' and the 'U') and letter shape ('E'/'U' for both Global and Local levels). This finding implies that the V1 network topologies were very stable across the individuals in the experiment. All these specific classifications ultimately depend on the patterns of retinotopic stimulation, which were highly distinguishable.

Second, intra-subject cross-classification was also accurate for the abstract level, transferring learning across letters identities. Both cross-classifications depend on information not strictly tied to the retinotopic pattern of stimulation (Kaplan et al., 2015; Valdés-Sosa et al., 2020); they are somewhat more abstract than for the specific discriminations. In the case of invariance for level, this implies that the details of line configurations distinguishing 'E' and 'U' were abstracted away (Hübner & Volberg, 2005). Shifting attention towards the Local/Global is thought to occur by filtering out high/low spatial frequencies from the representation of the retinal input. (Flevaris et al., 2011, 2014). In a prior study by our group using activation-based MVPA (Valdés-Sosa et al., 2020), information about level (independent from shape) was found in scene-selective cortex (medial ventral occipitotemporal and middle occipital areas). This area could be a source of feedback contributing to the intra-V1 network effect of level.

bioRxiv preprint doi: https://doi.org/10.1101/2022.10.20.513108; this version posted October 21, 2022. The copyright holder for this preprint (which was not certified by peer review) is the author/funder, who has granted bioRxiv a license to display the preprint in perpetuity. It is made available under aCC-BY-NC-ND 4.0 International license.

Transfer of learning did not occur for the invariant shape across different levels: cross-classification for letter identity failed. However, coding of shape that is tolerant to changes in size is present in higher-order-visual areas such as LOC (Grill-Spector, 2003). In our previous study, information about shape invariant with respect to level was found in these same object-selective cortices (lateral ventral occipitotemporal and lateral occipital regions, including LOC) (Valdés-Sosa et al., 2020). So why did the invariant classification of letter identity fail? One explanation of our results is that these size-invariant representations do not influence intra-V1 networks by feedback. However, this idea contradicts several studies showing robust functional connectivity between the foveal region of V1 and LOC (e.g., Baldassano et al., 2016). However, since the coupling between early and higher-order visual areas is selectively switched on or off according to task requirements (e.g., Al-aidroos et al., 2012), this would imply that in our task connections of V1 to areas controlling the spatial scale of attention would be enhanced on and those implicated with shape attenuated. When processing Navon figures, the control of spatial scale is essential (Flevaris & Robertson, 2016).

Edge HTW maps of this cross-classifier for level had different topologies when 'weighing in' for each level. For weights indicating Global stimuli, many links crossed the vertical meridian in the lower visual field. For weights indicating Local stimuli links were limited to single quadrants (especially the lower ones), with only a few crossings of the horizontal meridian. These results provide converging evidence for the previous work of our group using the same data but based on hypothesis testing using mass univariate edgewise and network-based statistics. Again we conclude that feedback influences are probable drivers of the intra-V1 networks since examination of these HTW shows that most discriminative links are longer than 4 degrees of visual angle, which exceeds the size of V1 receptive fields in the stimulated region.

bioRxiv preprint doi: https://doi.org/10.1101/2022.10.20.513108; this version posted October 21, 2022. The copyright holder for this preprint (which was not certified by peer review) is the author/funder, who has granted bioRxiv a license to display the preprint in perpetuity. It is made available under aCC-BY-NC-ND 4.0 International license.

The fact that the classifier weight maps described here and the significant links of our previous study both show stronger interhemispheric connections associated with Global stimuli in the lower visual field is consistent with evidence that Global visual perception is more accurate in the lower compared to the upper VF (Christman, 1993; Levine & McAnany, 2005; Previc, 1990). This advantage could be explained by greater sensitivity in the lower visual field to lower spatial frequency components (Niebauer & Christman, 1998), which are needed to extract Global shapes, including those in Navon figures (Flevaris & Robertson, 2016).

The demonstration that network patterns cross-validate across participants is not a trivial result, given the current concern about the reliability of hypothesis testing based on small samples (Calhoun, 2022). However, surviving this additional test is not enough, and higher-powered replications are needed, given the possibility of false positive results and inflated effect sizes in results from small samples (Button et al., 2013). Another limitation of this study is the lack of control of eye movements. Eye movements produce uncontrolled blurring of the retinotopic stimulus representation, which could weaken the correspondence of topologies across participants. Also, a small range of stimulus shapes was used. These problems must be addressed in replication studies with a larger number of stimuli and participants and with the measurement of eye movements.

Despite these limitations, this study bolsters our previous report based on hypothesis testing by using MVPA. Testing invariance of cortical information with simple hypothesis testing is impossible and can only be achieved by the cross-classification technique used here or by more sophisticated and recently developed multivariate analysis of variance methods (Allefeld & Haynes, 2014). The visual pathways are essentially machines for extracting important attributes disregarding other less critical features. Therefore, it is crucial to determine their possible feedback influence on V1. The cross-classification results indicate

bioRxiv preprint doi: https://doi.org/10.1101/2022.10.20.513108; this version posted October 21, 2022. The copyright holder for this preprint (which was not certified by peer review) is the author/funder, who has granted bioRxiv a license to display the preprint in perpetuity. It is made available under aCC-BY-NC-ND 4.0 International license.

that the relative weight of feedback influences from different higher-order visual regions on intra-V1 networks will shift according to the task. This hypothesis could be tested with mediation analyses using time series from higher-order visual areas as control variables.

Intersubject classification based on functional connectivity is promising for possible applications in medical diagnosis (Finn & Rosenberg, 2021; Serin et al., 2021; Tian & Zalesky, 2021). Intersubject cross-classifiers (e.g., for level) can be used to characterize individuals. In several neuropsychiatric disorders, global/local attention breaks down (Slavin et al., 2002; White et al., 2009). Would atypical intra-V1 networks emerge in patients affected when observing our modified Navon stimuli? This research could perhaps help characterize their neural physiopathology.

As a final point, we underline that our results are congruent with studies using MVPA on fMRI activations, revealing that V1 carries visual information with a spatial range more extensive than its pRFs (Smith & Muckli, 2010; Williams et al., 2008). Together, they support the hypothesis of V1 as a "cognitive blackboard" V1 (Roelfsema & de Lange, 2016), which could play an essential role in cognitive processes such as perceptual organization, attention, and memory.

bioRxiv preprint doi: https://doi.org/10.1101/2022.10.20.513108; this version posted October 21, 2022. The copyright holder for this preprint (which was not certified by peer review) is the author/funder, who has granted bioRxiv a license to display the preprint in perpetuity. It is made available under aCC-BY-NC-ND 4.0 International license.

References

Al-aidroos, N., Said, C. P., & Turk-browne, N. B. (2012). *Top-down attention switches coupling between low- Level and high-level areas of human visual cortex*. *109*(36), 14675–14680. https://doi.org/10.1073/pnas.1202095109

Allefeld, C., & Haynes, J. D. (2014). Searchlight-based multi-voxel pattern analysis of fMRI by cross-validated MANOVA. *NeuroImage*, *89*, 345–357. https://doi.org/10.1016/j.neuroimage.2013.11.043

Baldassano, C., Fei-Fei, L., & Beck, D. M. (2016). Pinpointing the peripheral bias in neural scene processing networks during natural viewing. *Journal of Vision*, *16*(2), 9. https://doi.org/10.1167/16.2.9.doi

Baldassano, C., Iordan, M. C., Beck, D. M., & Fei-Fei, L. (2012). Voxel-level functional connectivity using spatial regularization. *NeuroImage*, *63*(3), 1099–1106. https://doi.org/10.1016/j.neuroimage.2012.07.046

Behzadi, Y., Restom, K., Liau, J., & Liu, T. T. (2007). A component based noise correction method (CompCor) for BOLD and perfusion based fMRI. *NeuroImage*, *37*(1), 90–101. https://doi.org/10.1016/j.neuroimage.2007.04.042

Benson, N. C., Butt, O. H., Datta, R., Radoeva, P. D., Brainard, D. H., & Aguirre, G. K. (2012). The retinotopic organization of striate cortex is well predicted by surface topology. *Current Biology : CB*, *22*(21), 2081–2085. https://doi.org/10.1016/j.cub.2012.09.014

Benson, N. C., & Winawer, J. (2018). Bayesian analysis of retinotopic maps. *ELife*, *7*, 1–29. https://doi.org/10.7554/elife.40224

Button, K. S., Ioannidis, J. P. a, Mokrysz, C., Nosek, B. a, Flint, J., Robinson, E. S. J., & Munafò, M. R. (2013). Power failure: why small sample size undermines the reliability

bioRxiv preprint doi: https://doi.org/10.1101/2022.10.20.513108; this version posted October 21, 2022. The copyright holder for this preprint (which was not certified by peer review) is the author/funder, who has granted bioRxiv a license to display the preprint in perpetuity. It is made available under aCC-BY-NC-ND 4.0 International license.

of neuroscience. *Nature Reviews. Neuroscience*, *14*(5), 365–376. https://doi.org/10.1038/nrn3475

Bzdok, D., & Ioannidis, J. P. A. (2019). Exploration, Inference, and Prediction in Neuroscience and Biomedicine. *Trends in Neurosciences*, *42*(4), 251–262. https://doi.org/10.1016/j.tins.2019.02.001

Calhoun, V. D. (2022). *Reproducibility and replicability in neuroimaging data analysis*. 475–481. https://doi.org/10.1097/WCO.0000000000001081

Christman, S. D. (1993). Local-global processing in the upper versus lower visual fields. *Bulletin of the Psychonomic Society*, *31*(4), 275–278. https://doi.org/10.3758/BF03334927

Davis, T., & Poldrack, R. a. (2013). Measuring neural representations with fMRI: practices and pitfalls. *Annals of the New York Academy of Sciences*, 1–27. https://doi.org/10.1111/nyas.12156

Dawson, D. A., Lam, J., Lewis, L. B., Carbonell, F. M., Mendola, J. D., & Shmuel, A. (2016). Partial Correlation-Based Retinotopically Organized Resting-State Functional Connectivity Within and Between Areas of the Visual Cortex Reflects More Than Cortical Distance. *Brain Connectivity*, *6*(1), 57–75. https://doi.org/10.1089/brain.2014.0331

Finn, E. S. (2021). Is it time to put rest to rest? *Trends in cognitive sciences*, *25*(12), 1021-1032. https://doi.org/10.1016/j.tics.2021.09.005

Finn, E. S., & Rosenberg, M. D. (2021). Beyond fingerprinting: Choosing predictive connectomes over reliable connectomes. *NeuroImage*, *239*(June), 118254. https://doi.org/10.1016/j.neuroimage.2021.118254

bioRxiv preprint doi: https://doi.org/10.1101/2022.10.20.513108; this version posted October 21, 2022. The copyright holder for this preprint (which was not certified by peer review) is the author/funder, who has granted bioRxiv a license to display the preprint in perpetuity. It is made available under aCC-BY-NC-ND 4.0 International license.

Flevaris, A. v., Bentin, S., & Robertson, L. C. (2011). Attentional selection of relative SF mediates global versus local processing: Evidence from EEG. *Journal of Vision*, *11*(7), 1–12. https://doi.org/10.1167/11.7.1

Flevaris, A. v, Martínez, A., & Hillyard, S. A. (2014). Attending to global versus local stimulus features modulates neural processing of low versus high spatial frequencies: an analysis with event-related brain potentials. *Frontiers in Psychology*, *5*(April), 1–11. https://doi.org/10.3389/fpsyg.2014.00277

Flevaris, A. v., & Robertson, L. C. (2016). Spatial frequency selection and integration of global and local information in visual processing: A selective review and tribute to Shlomo Bentin. *Neuropsychologia*, *83*, 192–200. https://doi.org/10.1016/j.neuropsychologia.2015.10.024

Grill-Spector, K. (2003). The neural basis of object perception. *Current Opinion in Neurobiology*, *13*(2), 159–166. https://doi.org/10.1016/S0959-4388(03)00040-0

Haak, K. v., Winawer, J., Harvey, B. M., Renken, R., Dumoulin, S. O., Wandell, B. A., & Cornelissen, F. W. (2013). Connective field modeling. *NeuroImage*, *66*, 376–384. https://doi.org/10.1016/j.neuroimage.2012.10.037

Han, S., & Humphreys, G. W. (1999). Interactions between perceptual organization based on Gestalt laws and those based on hierarchical processing. *Perception & Psychophysics*, *61*(7), 1287–1298. https://doi.org/10.3758/BF03206180

Han, S., & Humphreys, G. W. (2002). Segmentation and selection contribute to local processing in hierarchical analysis. *Quarterly Journal of Experimental Psychology Section A: Human Experimental Psychology*, *55*(1), 5–21. https://doi.org/10.1080/02724980143000127

Haufe, S., Meinecke, F., Görgen, K., Dähne, S., Haynes, J. D., Blankertz, B., & Bießmann, F. (2014). On the interpretation of weight vectors of linear models in multivariate

bioRxiv preprint doi: https://doi.org/10.1101/2022.10.20.513108; this version posted October 21, 2022. The copyright holder for this preprint (which was not certified by peer review) is the author/funder, who has granted bioRxiv a license to display the preprint in perpetuity. It is made available under aCC-BY-NC-ND 4.0 International license.

neuroimaging. *NeuroImage*, *87*, 96–110. https://doi.org/10.1016/j.neuroimage.2013.10.067

Haynes, J.-D., & Rees, G. (2006). Decoding mental states from brain activity in humans. *Nature Reviews Neuroscience*, *7*(7), 523–534. https://doi.org/10.1038/nrn1931

Hübner, R., & Volberg, G. (2005). The integration of object levels and their content: a theory of global/local processing and related hemispheric differences. *Journal of Experimental Psychology. Human Perception and Performance*, *31*(3), 520–541. https://doi.org/10.1037/0096-1523.31.3.520

Iglesias-Fuster, J., Santos-Rodríguez, Y., Trujillo-Barreto, N., & Valdés-Sosa, M. J. (2014). Asynchronous presentation of global and local information reveals effects of attention on brain electrical activity specific to each level. *Frontiers in Psychology*, *5*(OCT), 1–14. https://doi.org/10.3389/fpsyg.2014.01570

Kaplan, J. T., Man, K., & Greening, S. G. (2015). Multivariate cross-classification: applying machine learning techniques to characterize abstraction in neural representations. *Frontiers in Human Neuroscience*, *9*(March), 1–12. https://doi.org/10.3389/fnhum.2015.00151

Lamme, V. A. F., & Roelfsema, P. R. (2000). The distinct modes of vision offered by feedforward and recurrent processing. *Trends in Neurosciences*, *23*(11), 571–579. https://doi.org/10.1016/S0166-2236(00)01657-X

Levine, M. W., & McAnany, J. J. (2005). The relative capabilities of the upper and lower visual hemifields. *Vision Research*, *45*(21), 2820–2830. https://doi.org/10.1016/j.visres.2005.04.001

Liang, H., Gong, X., Chen, M., Yan, Y., Li, W., & Gilbert, C. D. (2017). Interactions between feedback and lateral connections in the primary visual cortex. *Proceedings of*

bioRxiv preprint doi: https://doi.org/10.1101/2022.10.20.513108; this version posted October 21, 2022. The copyright holder for this preprint (which was not certified by peer review) is the author/funder, who has granted bioRxiv a license to display the preprint in perpetuity. It is made available under aCC-BY-NC-ND 4.0 International license.

the National Academy of Sciences of the United States of America, *114*(32), 8637–8642. https://doi.org/10.1073/pnas.1706183114

Nasr, S., Kleinfeld, D., & Polimeni, J. R. (2021). The Global Configuration of Visual Stimuli Alters Co-Fluctuations of Cross-Hemispheric Human Brain Activity. *The Journal of Neuroscience*, *41*(47), 9756–9766. https://doi.org/10.1523/jneurosci.3214-20.2021

Niebauer, C. L., & Christman, S. D. (1998). Upper and lower visual field differences in categorical and coordinate judgments. *Psychonomic Bulletin and Review*, *5*(1), 147–151. https://doi.org/10.3758/BF03209471

Previc, F. H. (1990). Functional specialization in the lower and upper visual fields in humans: Its ecological origins and neurophysiological implications. *Behavioral and Brain Sciences*, *13*(3), 519–542. https://doi.org/10.1017/S0140525X00080018

Roelfsema, P. R., & de Lange, F. P. (2016). Early Visual Cortex as a Multiscale Cognitive Blackboard. *Annual Review of Vision Science*, *2*, 131–151. https://doi.org/10.1146/annurev-vision-111815-114443

Saenz, M., & Fine, I. (2010). Topographic organization of V1 projections through the corpus callosum in humans. *NeuroImage*, *52*(4), 1224–1229. https://doi.org/10.1016/j.neuroimage.2010.05.060

Schaefer, A., Kong, R., Gordon, E. M., Laumann, T. O., Zuo, X.-N., Holmes, A. J., Eickhoff, S. B., & Yeo, B. T. T. (2018). Local-Global Parcellation of the Human Cerebral Cortex from Intrinsic Functional Connectivity MRI. *Cerebral Cortex*, *28*(9), 3095–3114. https://doi.org/10.1093/cercor/bhx179

Seidemann, E., & Geisler, W. S. (2018). Linking V1 Activity to Behavior. *Annual Review of Vision Science*, *4*(June), 287–310. https://doi.org/10.1146/annurev-vision-102016-061324

bioRxiv preprint doi: https://doi.org/10.1101/2022.10.20.513108; this version posted October 21, 2022. The copyright holder for this preprint (which was not certified by peer review) is the author/funder, who has granted bioRxiv a license to display the preprint in perpetuity. It is made available under aCC-BY-NC-ND 4.0 International license.

Serin, E., Zalesky, A., Matory, A., Walter, H., & Kruschwitz, J. D. (2021). NBS-Predict: A prediction-based extension of the network-based statistic. *NeuroImage*, *244*(October), 118625. https://doi.org/10.1016/j.neuroimage.2021.118625

Slavin, M. J., Mattingley, J. B., Bradshaw, J. L., & Storey, E. (2002). Local-global processing in Alzheimer's disease: an examination of interference, inhibition and priming. *Neuropsychologia*, *40*(8), 1173–1186. https://doi.org/10.1016/S0028-3932(01)00225-1

Smith, F. W., & Muckli, L. (2010). Nonstimulated early visual areas carry information about surrounding context. *Proceedings of the National Academy of Sciences of the United States of America*, *107*(46), 20099–20103. https://doi.org/10.1073/pnas.1000233107

Sporns, O., & Betzel, R. F. (2016). Modular brain networks. *Annual Review of Psychology*, *67*(September 2015), 613–640. https://doi.org/10.1146/annurev-psych-122414-033634

Tian, Y., & Zalesky, A. (2021). Machine learning prediction of cognition from functional connectivity: Are feature weights reliable? *NeuroImage*, *245*(May), 118648. https://doi.org/10.1016/j.neuroimage.2021.118648

Valdés-Sosa, M., Ontivero-Ortega, M., Iglesias-Fuster, J., Lage-Castellanos, A., Gong, J., Luo, C., Castro-Laguardia, A. M., Bobes, M. A., Marinazzo, D., & Yao, D. (2020). Objects seen as scenes: Neural circuitry for attending whole or parts. *NeuroImage*, *210*. https://doi.org/10.1016/j.neuroimage.2020.116526

Valdes-Sosa, M. J., Ontivero-Ortega, M., Iglesias-Fuster, J., Lage-Castellanos, A., Galan-Garcia, L., & Valdes-Sosa, P. A. (2022). Co-fluctuations of neural activity define intra-V1 networks related to perceptual organization. bioRxiv. https://doi.org/10.1016/j.neuroimage.2020.116526

Valente, G., Castellanos, A. L., Hausfeld, L., de Martino, F., & Formisano, E. (2021). Cross-validation and permutations in MVPA: Validity of permutation strategies and power of

bioRxiv preprint doi: https://doi.org/10.1101/2022.10.20.513108; this version posted October 21, 2022. The copyright holder for this preprint (which was not certified by peer review) is the author/funder, who has granted bioRxiv a license to display the preprint in perpetuity. It is made available under aCC-BY-NC-ND 4.0 International license.

cross-validation schemes. *NeuroImage*, *238*, 118145. https://doi.org/10.1016/j.neuroimage.2021.118145

Wandell, B. A., & Winawer, J. (2011). Imaging retinotopic maps in the human brain. *Vision Research*, *51*(7), 718–737. https://doi.org/10.1016/j.visres.2010.08.004

Wandell, B. A., & Winawer, J. (2015). Computational neuroimaging and population receptive fields. *Trends in Cognitive Sciences*, *19*(6), 349–357. https://doi.org/10.1016/j.tics.2015.03.009

Wang, Q., Cagna, B., Chaminade, T., & Takerkart, S. (2020). Inter-subject pattern analysis: A straightforward and powerful scheme for group-level MVPA. *NeuroImage*, *204*(September 2019), 116205. https://doi.org/10.1016/j.neuroimage.2019.116205

White, S., O'Reilly, H., & Frith, U. (2009). Big heads, small details and autism. *Neuropsychologia*, *47*(5), 1274–1281. https://doi.org/10.1016/j.neuropsychologia.2009.01.012

Williams, M. A., Baker, C. I., op de Beeck, H. P., Mok Shim, W., Dang, S., Triantafyllou, C., & Kanwisher, N. (2008). Feedback of visual object information to foveal retinotopic cortex. *Nature Neuroscience*, *11*(12), 1439–1445. https://doi.org/10.1038/nn.2218

bioRxiv preprint doi: https://doi.org/10.1101/2022.10.20.513108; this version posted October 21, 2022. The copyright holder for this preprint (which was not certified by peer review) is the author/funder, who has granted bioRxiv a license to display the preprint in perpetuity. It is made available under aCC-BY-NC-ND 4.0 International license.

Author contributions

Designed research: MOO, MVS, JIF

Contributed analytic tools: MOO, MVS, DM

Analyzed data: MOO, MVS

Wrote the paper: MOO, MVS

Competing Interests

The authors declare no competing interests.

Acknowledgements

This work was supported by the VLIR-UOS project "A Cuban National School of Neurotechnology for Cognitive Aging", and the National Fund for Science and Innovation of Cuba.